

Random-Phase Approximation in Many-Body Noncovalent Systems: Methane in a Dodecahedral Water Cage

Marcin Modrzejewski,^{*,†,‡} Sirous Yourdkhani,^{*,‡} Szymon Śmiga,[¶] and Jiří Klimeš^{*,‡}

[†]*Faculty of Chemistry, University of Warsaw, 02-093 Warsaw, Pasteura 1, Poland*

[‡]*Department of Chemical Physics and Optics, Faculty of Mathematics and Physics, Charles University, Ke Karlovu 3, CZ-12116 Prague 2, Czech Republic*

[¶]*Institute of Physics, Faculty of Physics, Astronomy and Informatics, Nicolaus Copernicus University, Grudziądzka 5, 87-100 Toruń, Poland*

E-mail: m.m.modrzejewski@gmail.com; yourdkhani.sirous@karlov.mff.cuni.cz;
klimes@karlov.mff.cuni.cz

Abstract

Molecular clusters are suitable systems for understanding the accuracy of theoretical methods. This is because their binding energy can be obtained both directly and using many-body expansion, allowing a detailed analysis. In this regard, the interaction between methane molecule and enclosing dodecahedral water cage represents a challenging test for electronic structure methods. To date, no hybrid or semilocal density-functional approximation has successfully accounted for the nonadditive contributions to the methane binding energy. Here we use many-body expansion to analyze the accuracy of the post-Kohn-Sham random-phase approximation (RPA) for the interaction energy of clathrate. This analysis reveals a crucial importance of the renormalized singles energy (RSE) corrections. RSE improves significantly the two-body contributions when used with standard generalized gradient approximation (GGA), meta-GGA, and their hybrids as well as for RPA based on optimized effective potential eigenstates. Remarkably, the inclusion of singles can also correct wrong signs of three- and four-body nonadditive energies as

well as mitigate excessive higher-order contributions to the many-body expansion. We find that the RPA errors are dominated by contributions of compact clusters and, as a way to improve the accuracy, we propose to replace these contributions by CCSD(T) energies. For RPA(PBE0) with RSE included it suffices to apply CCSD(T) to dimers and 30 trimers with hydrogen-bonded molecules (out of total 190 trimers) to get the methane–water cage interaction energy to within 1.6 % of the reference value.

1 Introduction

Datasets of interaction energies of molecular dimers are widely used to assess the accuracy of quantum chemistry methods for noncovalent interactions.^{1–4} How the methods perform for nonadditive interactions, that is, interactions involving three or more molecules with pairwise contributions removed, has gained much less attention.^{5–7} However, it was shown that three-body nonadditive interactions make an important contribution to the binding energies of atomic and molecular solids.^{8–10} Therefore, a reliable description of many-body interac-

tions is a clear aim in the development of low-scaling methods for large clusters and molecular solids.⁵

The three-body nonadditive energies pose a challenge to current density functional theory (DFT) approximations. In fact, approximate exchange functionals can deteriorate the three-body energies more than the missing description of three-body dispersion.^{7,11,12} One way to improve the results is to use a scheme that does not approximate electron exchange, such as the random-phase approximation (RPA). RPA is based on the frequency-dependent density response function built from DFT orbitals and orbital energies.¹³ Due to the account of n -body dispersion, RPA’s description of molecular solids⁶ and large clusters¹⁴ is more adequate than that of commonly used second-order Møller-Plesset perturbation theory (MP2). At the same time, low-scaling implementations promise routine use of RPA for molecular clusters and solids.^{15–21} We have recently shown²¹ that three-body RPA nonadditive interactions critically depend on the input DFT orbitals and the use of the renormalized singles energy (RSE).^{22,23} For example, RSE qualitatively improves the three-body energies for RPA based on PBE or PBE0 orbitals, but the SCAN-based results are affected less.²¹

Methane clathrate, modeled either as a finite cluster²⁴ or as a bulk material,²⁵ has been found to be a severe test case for widely used theoretical methods. Specifically, it is problematic to obtain accurately the interaction energy of methane molecule with the surrounding water cage. For bulk clathrate, Cox *et al.*²⁵ found that none of tested DFT methods, including nonlocal van der Waals functionals, correctly describes both the methane binding energy and lattice constants of the clathrate. The lack of reliable description of nonadditive interactions is one of the main causes of errors. For a clathrate cage model Deible *et al.*²⁴ showed that DFT models provide inaccurate predictions of three-body nonadditive energies ranging from -2.79 kcal/mol for BLYP²⁶ to 7.53 kcal/mol for PBE.²⁷

Here we use the methane clathrate cage model, $\text{CH}_4(\text{H}_2\text{O})_{20}$, to examine the accuracy

of different RPA approaches for predicting the interaction energy between methane and water cage. We analyze the importance of the RSE corrections and how is the RPA accuracy affected by the choice of DFT functional used to provide the input eigenstates for RPA. To understand the results in detail we have performed a many-body expansion of the interaction energy. This shows, for example, considerable error cancellation between three- and four-body energies for RPA based on the PBE functional, which is almost removed when the RSE corrections are used. In contrast, RPA calculations employing SCAN orbitals do not suffer from such deficiencies.

To assess the quality of RPA we have obtained reference many-body contributions up to tetramers using the coupled cluster scheme with singles, doubles, and perturbative triples excitations (CCSD(T)) leading to total interaction energy of -4.71 kcal/mol. The value differs from the estimate of Deible *et al.*, $E_{\text{int}} = -5.3 \pm 0.5$ kcal/mol,²⁴ likely due to the stochastic uncertainty of diffusion Monte Carlo and other uncertainties.²⁸ More recently, Lao and Herbert²⁹ have employed domain-based local pair natural orbital CCSD(T) approach (DLPNO-CCSD(T))^{30,31} and obtained an interaction energy of -4.88 kcal/mol which is more consistent with our result. We note that the calculation of the reference value involves calculations of 20 dimers, 190 trimers, and 1140 tetramers. The large number of tetramers represents a considerable computational effort. Therefore, to guide the use of more efficient methods in the future, we test a strategy where we start from the RPA interaction energy of the whole cage with methane, and perform the many-body expansion on the difference between CCSD(T) and RPA. We find that with this incremental scheme one only needs to perform CCSD(T) calculations of dimers and 30 trimers with hydrogen-bonded water molecules to obtain the interaction energy to within 0.08 kcal/mol (around 1.6%) of the reference value.

2 Methods

Within the many-body expansion approach the methane molecule in a dodecahedral water cage is treated as cluster of $N = 21$ molecules. The total interaction energy is assembled from n -body contributions, where each n -body fragment includes methane:

$$E_{\text{int}} = E_{\text{int}}[2] + E_{\text{int}}[3] + E_{\text{int}}[4] + \dots \quad (1)$$

$$E_{\text{int}}[2] = \sum_{i=1}^{20} E_{\text{int}}(0, i) \quad (2)$$

$$E_{\text{int}}[3] = \sum_{i=1}^{19} \sum_{j=i+1}^{20} E_{\text{int}}(0, i, j) \quad (3)$$

$$E_{\text{int}}[4] = \sum_{i=1}^{18} \sum_{j=i+1}^{19} \sum_{k=j+1}^{20} E_{\text{int}}(0, i, j, k) \quad (4)$$

The indices i, j, k, \dots denote the individual water molecules; 0 corresponds to the methane molecule. The brackets are dropped from the notation when no ambiguity arises. $E_{\text{int}}(0, i)$ denotes the dimer interaction energy of methane and i th water

$$E_{\text{int}}(0, i) = E(0, i) - E(0) - E(i) \quad (5)$$

The higher-order terms are the nonadditive interaction energies of individual trimers

$$\begin{aligned} E_{\text{int}}(0, i, j) &= E(0, i, j) \\ &\quad - E(0) - E(i) - E(j) \\ &\quad - E_{\text{int}}(0, i) - E_{\text{int}}(0, j) - E_{\text{int}}(i, j) \end{aligned} \quad (6)$$

and tetramers

$$\begin{aligned} E_{\text{int}}(0, i, j, k) &= E(0, i, j, k) \\ &\quad - E(0) - E(i) - E(j) - E(k) \\ &\quad - E_{\text{int}}(0, i) - E_{\text{int}}(0, j) - E_{\text{int}}(0, k) \\ &\quad - E_{\text{int}}(i, j) - E_{\text{int}}(i, k) - E_{\text{int}}(j, k) \\ &\quad - E_{\text{int}}(0, i, j) - E_{\text{int}}(0, i, k) \\ &\quad - E_{\text{int}}(0, j, k) - E_{\text{int}}(i, j, k) \end{aligned} \quad (7)$$

The energy of geometry relaxation is not included, i.e., the coordinates are fixed at their cluster values. All energies contributing to an n -body term are computed in the basis set of the corresponding n -body cluster. We com-

pare the different choices of basis sets below in Sec. 3.1.5. The explicit many-body expansion includes all clusters up to tetramers: 20 dimers, 190 trimers, and 1140 tetramers.

In the text and tables, we refer to the set of all n -body clusters using the label nb . Furthermore, the clusters with more than one water molecule are divided into subsets according to the number of hydrogen bonds. The label of an n -body cluster with m hydrogen bonds is $nb\ m\text{hb}$. For example, the label corresponding to the tetramers $\text{CH}_4(\text{H}_2\text{O})_3$ having two hydrogen bonds is 4b 2hb.

For the Hartree-Fock, MP2, DFT, and RPA methods it is computationally possible to obtain the energy of the complete cluster. In such a case the interaction energy is obtained directly by subtracting the energies of methane and the water cage from the energy of the cluster. As the water cage is treated as a single fragment, this scheme is referred to as the supermolecular approach. The supermolecular interaction energy is also used to provide an estimate of five- and higher-body terms. The supermolecular calculations are carried out with the full counterpoise correction encompassing all centers in the complex.

The Hartree-Fock, Møller-Plesset, and coupled cluster calculations were done using Molpro.³² We used the augmented version of the correlation-consistent basis sets of Dunning and coworkers,^{33,34} which we denote by a shorthand $\text{AV}n\text{Z}$, where n is the cardinal number of the basis set. The correlation energy was extrapolated to the basis set limit using the formula of Halkier et al.³⁵ As an alternative, the explicitly correlated (F12) approach was used to speed-up the basis-set convergence of the coupled cluster and MP2 energies.³⁶⁻³⁸ For the mean-field methods, the interaction energy obtained with the largest basis set was directly used, without any extrapolation. For the explicitly correlated schemes, the Hartree-Fock basis-set incompleteness error was reduced by calculating the complete auxiliary basis set singles correction (CABS).^{37,39}

The large number of individual MBE contributions requires that they are computed with high precision. For Molpro calculations, the or-

bital and energy convergence criteria were set to at least 10^{-8} Hartree. Within MBE, only the F12 calculations used resolution of identity. The AVnZ/JKFIT,⁴⁰ AVnZ/MP2FIT,^{41,42} and AVnZ/OPTRI⁴³ basis sets were respectively used for exchange fitting, density fitting, and resolution of identity (the corresponding Molpro keywords `df_basis_exch`, `df_basis`, and `ri_basis`). Resolution of identity was used also in the HF and MP2 supermolecular calculations. The cardinal numbers of the auxiliary basis sets were larger by one compared to the orbital basis sets.

The post-Kohn Sham RPA calculations based on PBE, PBE0, SCAN, and SCAN0 were carried out with the cubic-scaling algorithm described in Ref. 21 and implemented in an in-house code. The n -body RPA interaction energy can be written down as follows:

$$E_{\text{int}}^{\text{RPA}} = E^{\text{HF}} + E_c^{\text{RPA}} \quad (8)$$

where E^{HF} is the Hartree-Fock-like energy expression evaluated on Kohn-Sham orbitals and E_c^{RPA} is the post-Kohn Sham direct RPA correlation energy. All terms on the right-hand side of Eq. 8 are energy differences computed according to Eqs. 5–7. The RPA interaction energy with the renormalized singles energy²³ (RSE) is analogous to Eq. 8 but includes the RSE term

$$E_{\text{int}}^{\text{RPA+RSE}} = E^{\text{HF}} + E_c^{\text{RSE}} + E_c^{\text{RPA}} \quad (9)$$

The RSE term is computed using the Hartree-Fock density matrix computed by diagonalization of the Fock matrix built from the Kohn-Sham orbitals.²³

$$E_c^{\text{RSE}} = \text{Tr} \left(\boldsymbol{\rho}^{\text{HF}} \mathbf{F}^{\text{HF}} \left[\boldsymbol{\rho}^{\text{DFT}} \right] \right) - \text{Tr} \left(\boldsymbol{\rho}^{\text{DFT}} \mathbf{F}^{\text{HF}} \left[\boldsymbol{\rho}^{\text{DFT}} \right] \right) \quad (10)$$

The RPA calculations with PBE, PBE0, SCAN, and SCAN0 orbitals employed the tightest set of numerical precision thresholds defined in Table 1 of Ref. 21. Unless noted otherwise, the RPA correlation energies were extrapolated to the complete basis-set limit with the basis sets AVTZ and AVQZ.³⁵ The Hartree-Fock compo-

nent and the renormalized singles energy were computed with the AVQZ basis without any extrapolation. The method used to optimize the grids for frequency and imaginary-time integrals was changed with respect to the previous work. In Ref. 21 the quadratures are optimized for distribution of orbital energy differences (d_{ai} in Ref. 21) occurring in the full n -body cluster (*e.g.*, a trimer) and all its subsystems. In this work, the quadrature optimization subroutine ignores the high energy differences which occur in the subsystems, but are above the largest occupied-virtual orbital energy difference in the full n -body cluster. This modification results in a smaller number of quadrature points, especially for tetramers, while having no discernible effect on numerical precision. As a result, the number of grid points is reduced for systems with a large number of ghost atoms.

The orbitals and orbital energies generated with the optimized effective potential (OEP) method, OEPX⁴⁴ and OEP2-sc,^{45–48} were computed in the uncontracted correlation-consistent basis sets with the ACES II program.⁴⁹ The post-Kohn-Sham RPA calculations based on the OEP orbitals were carried out with a modified version of the coupled-clusters code of Ref. 50. Following previous work reported in Refs. 45–47, the equations of the optimized effective potential (OEP) method were solved with the finite-basis set procedure of Refs. 51 and 52. To calculate the pseudo-inverse of the density-density response matrix, we utilized truncated singular value decomposition (TSVD). This step is essential for determining stable and physically meaningful OEP solutions.^{45,53,54} The cutoff threshold of TSVD was set to 10^{-6} . In all OEP calculations, we employed the same tight thresholds as in Ref. 50. We refer the reader to Ref. 45 for additional technical details.

3 Results

3.1 Many-body expansion reference values

We now discuss the many-body expansion of the interaction energy at the coupled cluster level. To obtain reliable reference interaction energy, *i.e.*, results with precision of one or two per cent, there are several critical issues to overcome. Most importantly, the values need to be converged with respect to the basis-set size and also with the order of MBE, *i.e.*, the number of molecules in the largest fragment. Moreover, for large clusters the individual contributions need to be obtained with a high precision.⁵⁵

To assess the convergence with the basis-set size, we compare results obtained with basis-set extrapolation procedures to data computed using explicitly correlated (F12) methods. The convergence with the basis-set size is the most critical for dimers and, fortunately, the nonadditive contributions of larger clusters converge much faster with the basis-set size.⁵⁶ Concerning the order of MBE, we computed explicit n -body terms up to clusters containing four molecules. To assess the importance of higher-order terms we have compared the results of MBE and of the supermolecular approach. For HF and MP2 they agree within a few hundredths of kcal/mol so that the fourth order MBE should be sufficiently converged.

3.1.1 Dimers

The largest contribution to the interaction energy comes from the twenty two-body terms involving the interaction between a single water molecule and methane. The CCSD(T) and CCSD(T)-F12 results are summarized in Table 1. We present values for all the basis sets used and, where applicable, also estimates of the basis-set limit obtained with the two-point formula of Halkier *et al.*³⁵

The total two-body Hartree-Fock contribution shows very little dependence on the basis-set size, changing by less than 0.01 kcal/mol between AVTZ and AV5Z basis sets. This is partly due to the cancellation of the basis-set er-

rors of the individual contributions. The CABS correction has little effect on $E_{\text{int}}[2]$ but improves the convergence of the individual terms. For example, adding CABS reduces the errors in the AVTZ basis set approximately by a factor of three.

As expected, the CCSD contribution shows stronger dependence on the basis-set size so that either extrapolation or the use of the F12 scheme is needed. The difference between the AVTZ \rightarrow AVQZ and AVQZ \rightarrow AV5Z estimates of the CCSD correlation energy is 0.028 kcal/mol. That difference is similar to the difference between CCSD-F12b energies obtained with AVTZ and AVQZ basis sets. The CCSD-F12b contribution then changes by a mere 0.006 kcal/mol upon going to the AV5Z basis set. We therefore assume that the CCSD-F12b value is closer to the CBS limit.

The perturbative triples (T) term shows also slow convergence with the basis set size so that extrapolation to the CBS limit is needed in the canonical approach. While there are no F12 corrections for triples, the triples term can be scaled with the ratio of MP2-F12 and MP2 correlation energies to achieve faster basis-set convergence.³⁸ Note, however, that there is a subtle point in how this is performed. One can either scale the monomer (T) energies independently or use the dimer scaling factor in all the calculations. Only the latter approach is size-consistent.⁵⁷ In practice, the differences between the approaches are small and for dimers there is no clear preference for a single scheme. In particular, there is a close agreement between the two-body (T) energy obtained with independent scaling and with unscaled (T) extrapolated using the AVQZ and AV5Z basis sets. This holds also for the individual contributions of the twenty dimers. Using a common scaling factor leads to a more attractive (T) contribution but there is also a larger change between the AVQZ basis set and AV5Z basis set compared to the independent scaling approach. To sum up, independent scaling or extrapolation work well and we take the unscaled (T) obtained by extrapolation as the reference value.

The total two-body contribution without and with the use of F12 is -6.33 kcal/mol

and -6.31 kcal/mol, respectively. Based on the basis-set convergence we deem the latter value to be more precise and estimate that its uncertainty is 0.01 kcal/mol. This excludes core correlation and correlation contributions beyond CCSD(T). Our value differs from -5.85 kcal/mol obtained by Deible and co-workers in Ref. 24. The reason is the use of the much smaller VTZ-F12 basis set in Ref. 24. The HF contributions obtained with the VTZ-F12 and AVTZ basis set differ by less than one cal/mol. However, in the VTZ-F12 basis-set the CCSD-F12b contribution equals -8.260 kcal/mol and the scaled and unscaled (T) contributions are -1.544 and -1.427 kcal/mol, respectively. These values differ considerably from the AVTZ data, see Table 1. Adding the HF, CCSD-F12b, and unscaled (T) contributions reproduces the value given in Ref. 24 so that the basis set is indeed the cause of the difference. The inferior performance of the VTZ-F12 basis set can be most likely attributed to the lack of diffuse functions.

3.1.2 Trimers

We now discuss the three-body nonadditive contributions to the interaction energy. The data for CCSD(T) and CCSD(T)-F12 are summarized in Table 2. For most of the components, there is almost no dependence on the basis-set size. For example, the total three-body contribution of canonical CCSD(T) obtained with the AVTZ basis-set differs only by around 0.01 kcal/mol from the data extrapolated to the CBS limit. When the F12 approach is used, CCSD-F12b values in the AVTZ and AVQZ basis sets are within one cal/mol.

The only term requiring attention is the triples (T) energy. The convergence of triples is fast with the basis set in the unscaled variant and when a common scaling factor is used. For example, unscaled (T) is essentially converged in the AVTZ basis set. By contrast, the convergence is slower when the (T) components are scaled independently in the monomer and dimer subsystems.

Overall, the reference total three-body contribution using the CCSD(T) method is

1.04 kcal/mol. The values taken to obtain this value are in bold fontface in Table 2. Our result agrees with the value of $E_{\text{int}}[3] = 1.01$ kcal/mol reported by Deible *et al.*,²⁴ which again demonstrates the weaker dependence of the three-body term on the basis-set size.

3.1.3 Tetramers

There are 1140 tetramers, many more compared to 20 dimers and 190 trimers, suggesting a much larger computational effort. However, given that the total three-body term differs by only 0.001 kcal/mol between the AVTZ and AVQZ basis sets, we expect that the four-body term will show similar behavior. We have therefore used the CCSD(T)-F12b scheme together with the AVTZ basis-set to obtain the four-body terms. Spot checks on twenty tetramers show that for CCSD-F12b the largest differences between the AVTZ and AVQZ data are on the order of 10^{-5} kcal/mol for a single tetramer. Since there are 1140 tetramers, the difference upon going to the AVQZ basis could be at most on the order of 10^{-2} kcal/mol. However, we expect it to be smaller as some of the individual contributions are positive and some negative. The weak dependence on the basis set size is also confirmed by tetramer calculations in the AVDZ basis set.

The CCSD(T)-F12b four-body energy and the contributions of the different components are shown in Table 3. The Hartree-Fock term dominates over the correlation part. As with the three-body terms, individual scaling of the triples should be avoided. Using a common scaling factor or doing no scaling of triples leads to a fast convergence with the basis set size.

The CCSD(T) interaction energy obtained up-to fourth order of MBE is -4.72 kcal/mol. We estimate the higher-order effects as the difference between supermolecular and MBE calculation at the Hartree-Fock level, which is 0.01 kcal/mol. Therefore, our final estimate of the CCSD(T) interaction energy between methane and the water cage is -4.71 kcal/mol. We estimate its uncertainty to be below one percent or 0.04 kcal/mol. The value nor its uncertainty include core correlations or correlation

Table 1: Two-body contributions to the coupled clusters interaction energy (kcal/mol). The contributions used in the final coupled-cluster reference are written in bold.

Method	AVTZ	AVQZ	AVTZ→AVQZ	AV5Z	AVQZ→AV5Z
HF ^a	3.836	3.832	—	3.828	—
CCSD ^b	-8.175	-8.388	-8.543	-8.450	-8.515
(T) ^c	-1.528	-1.597	-1.648	-1.618	-1.640
CCSD(T) ^d	-5.867	-6.153	-6.359	-6.240	-6.328
HF+CABS ^a	3.835	3.830	—	3.827	—
CCSD-F12b ^b	-8.467	-8.494	—	-8.500	—
(T) ^c _{unscaled}	-1.513	-1.589	-1.645	-1.614	-1.639
(T) ^{c,e} _{scaled}	-1.624	-1.637	—	-1.638	—
(T) ^{c,f} _{scaled}	-1.659	-1.655	—	-1.649	—
CCSD(T)-F12b ^g	-6.144	-6.252	-6.308	-6.286	-6.312

^a Hartree-Fock contribution to $E_{\text{int}}[2]$.

^b CCSD correlation-only contribution.

^c Correlation-only contribution of perturbative triples.

^d Sum of HF, CCSD, and (T) values. For AVTZ→AVQZ and AVQZ→AV5Z columns, HF data obtained with AVQZ and AV5Z basis sets were used, respectively.

^e Independent scaling factors for the dimer and monomers.

^f Common scaling factor for the dimer and monomers .

^g Obtained as a sum of HF+CABS, CCSD-F12b, and (T)_{unscaled} values, for AVTZ→AVQZ and AVQZ→AV5Z columns HF+CABS and CCSD-F12b values obtained with AVQZ and AV5Z basis sets were used, respectively.

beyond the (T) term. The uncertainty comes from basis-set convergence, possible loss of precision of the four-body terms,⁵⁵ and five-body and higher correlation contributions.

3.1.4 Møller-Plesset perturbation theory

Before we use the coupled cluster benchmark to assess RPA, we apply the Møller-Plesset hierarchy of methods to gain additional insight into the energy contributions. Both MP2 and MP3 underestimate the two-body term by approximately 1 kcal/mol (Table 4). MP4 performs much better and is within 0.05 kcal/mol of the reference value. There are two types of trimers, with and without hydrogen bonded water molecules, we denote them “3b 1hb” and “3b 0hb”, respectively. As discussed by Deible *et al.*, MP2 lacks three-body dispersion contributions and the total three-body term is too attractive for either of the groups. The MP3 and MP4 results are close to the reference values both for the hydrogen-bonded and non-hydrogen-bonded trimers. We note that a sim-

ple arithmetic mean of the MP2 and MP3 interaction energies (the MP2.5 approach) has been proposed to improve the interaction energies of dimers and nonadditive three-body energies of non-covalent clusters.^{5,58} Interestingly, this scheme would not improve the accuracy of MP3 for the three-body terms in clathrate.

The largest contributions to four-body correlation energy comes from the clusters with two hydrogen bonds. Here MP2 does not provide enough attractive correlation leading to too repulsive total four-body contribution (by 0.06 kcal/mol). MP3 does not bring an overall improvement compared to MP2, the errors are reduced for the 4b 0hb subset but the accuracy deteriorates for the 4b 1hb fragments. Interestingly, the total HF+CABS four-body contribution is within 0.01 kcal/mol of the CCSD(T) reference, which is a result of a fortunate cancellation of errors.

The total sum of the two-, three-, and four-body terms shows that both MP2 and MP3 underestimate the total interaction energy, mostly due too weakly binding two-body contributions. The aforementioned lack of three-body

Table 2: Three-body contributions to the coupled clusters interaction energy (kcal/mol). The contributions used in the final coupled-cluster reference are written in bold.

Method	AVTZ	AVQZ	AVTZ→AVQZ
HF ^a	-0.273	-0.273	—
CCSD ^b	1.112	1.108	1.106
(T) ^c	0.205	0.203	0.202
CCSD(T) ^d	1.044	1.039	1.035
HF+CABS ^a	-0.273	-0.272	—
CCSD-F12b ^b	1.106	1.106	—
(T) _{unscaled} ^c	0.201	0.202	0.202
(T) _{scaled} ^{c,e}	0.046	0.114	—
(T) _{scaled} ^{c,f}	0.221	0.210	—
CCSD(T)-F12b ^g	1.034	1.035	1.035

^a Hartree-Fock contribution to $E_{\text{int}}[3]$.

^b CCSD correlation-only contribution.

^c Correlation-only contribution of perturbative triples.

^d Sum of HF, CCSD, and (T) contributions, value in AVTZ→AVQZ column uses HF data obtained with AVQZ basis set.

^e (T) contributions scaled individually in each calculation.

^f Common scaling factor for (T) contributions.

^g Sum of HF+CABS, CCSD-F12b, and (T)_{unscaled} data, in AVTZ→AVQZ column the HF+CABS and CCSD-F12b results obtained with AVQZ basis set are used.

dispersion in MP2 partly cancels the error of two-body terms so that the overall error of MP2 (0.39 kcal/mol) is about one half of the MP3 one (0.91 kcal/mol). Approximating the four-body MP4 terms by HF values, we estimate its interaction energy to be approximately -4.83 kcal/mol, around 0.1 kcal/mol away from the reference value.

Interestingly, the trend of the MP2 errors for the three-body contributions is consistent with the Axilrod-Teller-Muto (ATM) formula for three-body dispersion.^{59,60} According to the ATM term, the three-body dispersion is attractive for linear configurations and repulsive for trimer angles below approximately 117°. The 3b 1hb configurations have structure similar to isosceles triangle with vertex angle around 40° and the ATM three-body dispersion term is repulsive. For these trimers MP2 recovers only around 50 % of the (repulsive) CCSD(T) correlation. For the same reason MP2 also overbinds the proximate 0hb trimers (formed by second nearest neighbor water molecules). With increasing distance between the water molecules

the trimer angle increases so that the error is around zero for third nearest neighbor waters and positive for trimers close to linear geometry, see SI and additional resources.⁶¹

3.1.5 Basis sets for fragment calculations

There is an ample body of literature devoted to the choice of basis sets for MBE calculations.^{56,62-68} This is because calculations in the basis set of the whole cluster quickly become prohibitive when the system size increases and a less demanding approach needs to be used. In this work, all $n \leq 4$ -body cluster calculations are done in the fragment-centered basis set, *e.g.*, the trimer basis set is used for all single-point energies contributing to a given trimer’s nonadditive energy. Let us compare this approach to an alternative approach which employs the full-cluster basis set.

MP2 and MP2-F12 dimer interaction energies in the dimer and full-cluster basis sets, with increasing cardinal numbers, are shown in Fig. 1.

Table 3: Four-body contributions to the coupled clusters interaction energy, data in kcal/mol. The contributions used in the final coupled-cluster reference are written in bold.

Method	AVDZ	AVTZ
HF+CABS ^a	0.548	0.552
CCSD-F12b ^b	-0.010	-0.016
(T) _{unscaled} ^c	0.019	0.021
(T) _{scaled} ^{c,d}	-1.480	0.895
(T) _{scaled} ^{c,e}	0.025	0.023
CCSD(T)-F12b ^f	0.557	0.557

^a Hartree-Fock contribution to $E_{\text{int}}[4]$.

^b CCSD correlation-only contribution.

^c Correlation-only contribution of perturbative triples.

^d (T) contributions scaled individually in each calculation.

^e Common scaling factor for (T) contributions.

^f Sum of HF+CABS, CCSD-F12b, and (T)_{unscaled} contributions.

Clearly both basis set types lead to the same CBS limit. The rate of convergence of the full-cluster energies is only marginally faster, while the calculations are much more computationally demanding. The difference between the full-cluster basis and fragment basis becomes even less important for the three-body contribution, as demonstrated in Fig. 2. Here the selected trimer belongs to the 3b 1hb subset. The difference between the MP2-F12 nonadditive energies in the full-cluster and trimer basis set is $< 2 \cdot 10^{-4}$ kcal/mol in the AVDZ basis set and an order of magnitude smaller than that for the AVTZ and AVQZ basis sets. We conclude that the n -body fragment-centered basis sets employed in this work for all explicit MBE terms do not introduce any considerable basis set error and require less computational effort compared to the cluster basis set.

3.2 Performance of RPA

3.3 Supermolecular approach

For medium size clusters, including the clathrate cluster, the RPA energy can be obtained within a single calculation using the

efficient cubic-scaling RPA algorithm.²¹ In Table 5 we present the interaction energies of methane with the water cage obtained using RPA based on two pure DFT functionals (PBE and SCAN) and their hybrid variants. From the data one could think that RPA is not much sensitive to the input eigenstates, the spread of the predicted interaction energies is only 0.56 kcal/mol. In agreement with our previous work, the PBE-based RPA binds the most while RPA(SCAN0) binds the least.²¹ Adding the singles corrections divides the results into two groups divided by around 1 kcal/mol and straddling the reference value. RPA+RSE based on pure functionals slightly overbinds while RPA+RSE based on hybrids binds too little due to less attractive RSE correction. However, the close agreement of the results is deceptive, especially for RPA based on PBE. One can see considerable differences between the different variants in the many-body expansion which we discuss in the following.

3.3.1 Dimers

The dimer interactions of $\text{CH}_4 \cdots \text{H}_2\text{O}$ are, among the investigated n -body terms, by far the most challenging contributions to be accounted for by RPA. The interaction energy decomposition has the characteristics of dispersion dominated systems: almost the entire binding comes from the dispersion contribution ($E_{\text{disp}}^{\text{SAPT2+3(CCD)}} = -11.55$ kcal/mol), which is largely balanced by the first-order exchange repulsion energy ($E_{\text{exch}} = 8.91$ kcal/mol), see Ref. 69 for the description of the SAPT2+3(CCD) scheme. As we have found in our previous work, the RPA energy of a system dominated by dispersion tends to be sensitive to the choice of the Kohn-Sham determinant.²¹ First, the repulsion becomes more pronounced when the orbitals overlap more. The repulsive component is thus prone to the excessive polarization of (meta-)GGAs. Second, as a narrowing energy gap decreases the energy denominators of the dynamic polarizability, the functionals which predict smaller gaps tend to yield more attractive energies.

Let us analyze the accumulated 20 dimer in-

Table 4: Contributions to the methane–water cage interaction energy divided into n -body terms (nb) and subsystems with m hydrogen bonds (mhb). Energies are in kcal/mol.

Method	2b	3b 1hb	3b 0hb	4b 2hb	4b 1hb	4b 0hb	Sum
HF+CABS ^a	3.827	-1.483	1.210	0.164	0.471	-0.083	4.107
CCSD-F12b ^b	-8.500	0.913	0.193	-0.093	0.054	0.023	-7.410
(T) ^c	-1.639	0.172	0.030	-0.015	0.027	0.009	-1.415
CCSD(T)-F12b ^d	-6.312	-0.398	1.434	0.056	0.552	-0.051	-4.718
MP2 ^e	-5.192	-0.956	1.208	0.117	0.563	-0.067	-4.326
MP3 ^e	-5.452	-0.382	1.501	0.077	0.519	-0.067	-3.803
MP4 ^e	-6.360	-0.433	1.409	—	—	—	—

^a Hartree-Fock contribution to $E_{\text{int}}[nb\ mhb]$.

^b CCSD-F12b correlation-only contribution.

^c Correlation-only contribution of perturbative triples, no scaling of triples used.

^d Sum of HF+CABS, CCSD-F12b, and (T) energy terms.

^e $E_{\text{int}}^{\text{MP}n} = E^{\text{HF}} + E_{\text{c}}^{\text{MP}n}$.

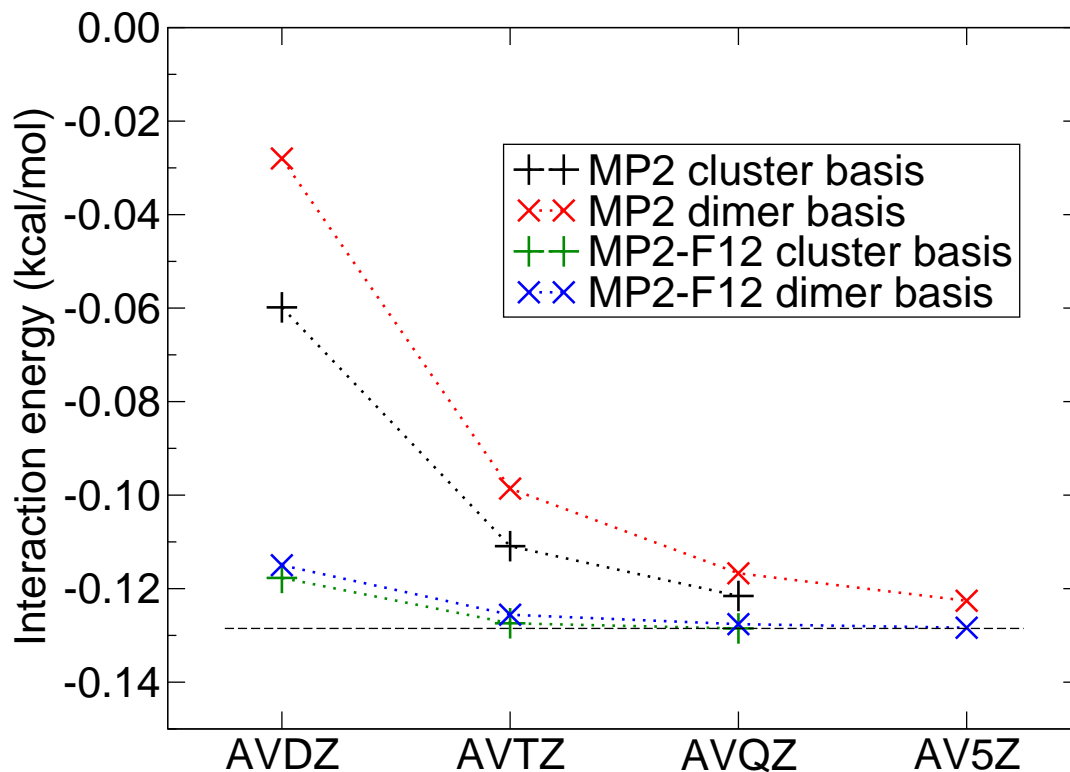


Figure 1: Interaction energy of water methane dimer obtained using basis set functions at every atom of $\text{CH}_4(\text{H}_2\text{O})_{20}$ (cluster basis) and basis set with functions centered on the interacting dimer only (dimer basis).

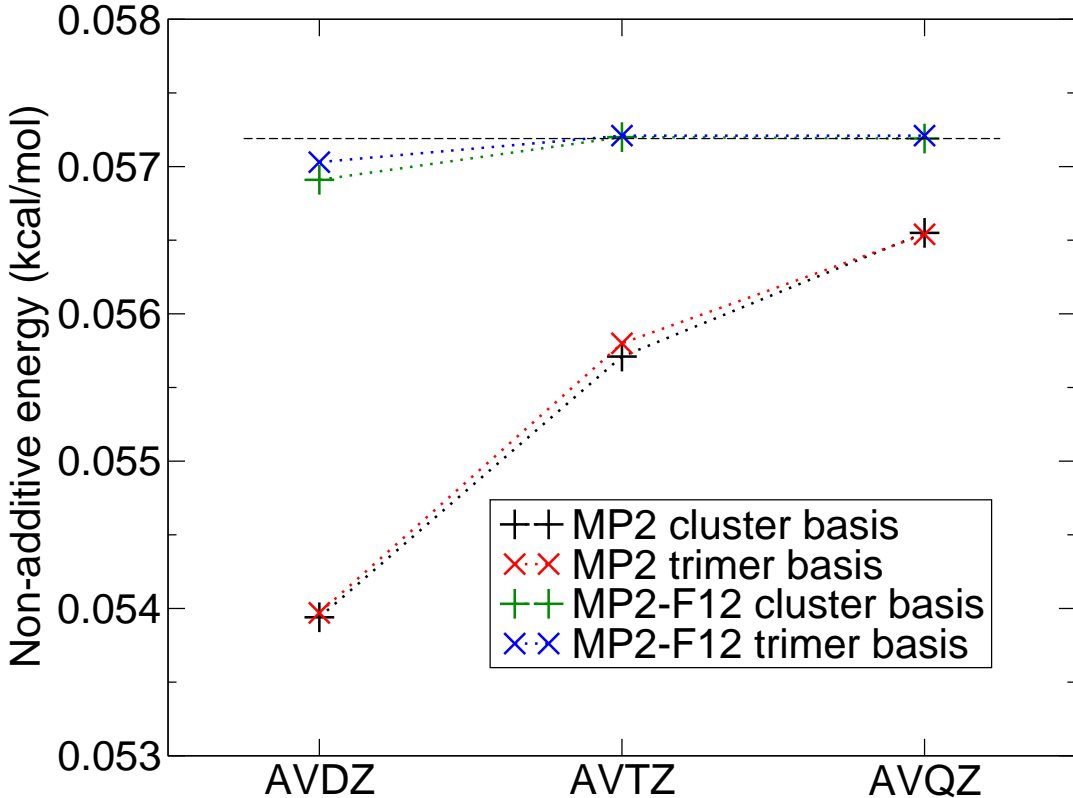


Figure 2: Three-body nonadditive energy of hydrogen-bonded water dimer with methane obtained using the full cluster basis and the trimer basis.

teraction energies in Table 6. (The individual dimer energies are available in the Supporting Information.) The repulsive interaction is accounted for in the Hartree-Fock energy contribution, E^{HF} , evaluated on a range of orbital inputs. Among pure and hybrid (meta-)GGAs, E^{HF} varies by over 2 kcal/mol, which is significant on the scale of the total interaction energy. In all cases the mean field contribution evaluated on DFT orbitals is considerably more repulsive than the self-consistent Hartree-Fock energy, by 1.5 to almost 3.9 kcal/mol. However, the differences are essentially expunged by the singles correction E_c^{RSE} . Except for the case of Hartree-Fock orbitals, the total mean-field contribution, $E^{\text{HF}} + E_c^{\text{RSE}}$, falls within a narrow range of 4.3–4.9 kcal/mol. This is only 0.5 to 1.0 kcal/mol larger than the self-consistent Hartree-Fock term $E^{\text{HF}} = 3.84$ kcal/mol.

Once E_c^{RSE} is added, the main source of differences among functionals is E_c^{RPA} . The large negative correlation contribution in pure (meta-)GGA variants, RPA(SCAN)+RSE and RPA(PBE)+RSE, leads to a small overbind-

ing in the total two-body energy, by 0.15 and 0.39 kcal/mol. In contrast, the methods based on hybrid functionals with 25% of exact exchange, RPA(SCAN0)+RSE and RPA(PBE0)+RSE, underestimate the two-body energy by as much as 1 kcal/mol.

Obviously the two sources of errors in our RPA treatment of methane-water dimers are the orbital input and the lack of the exchange-correlation kernel. It is worthwhile to investigate what level of accuracy can be achieved if one stays within the direct RPA framework, but uses high-quality orbitals. While the main focus remains on the PBE/SCAN-based exchange-correlation potentials, we briefly introduce a sequence of RPA variants based on increasingly sophisticated orbital inputs: from Hartree-Fock, to the exchange-only optimized effective potential (OEPX), to the optimized effective potential with second order correlation (OEP2-sc). By using ab initio DFT,⁷⁰ we factor out the influence of errors known to be present in the orbitals from semilocal exchange-correlation potentials, e.g., the excessive polar-

Table 5: Total methane—water cage interaction energy (kcal/mol).^a

	SCAN0	PBE0	SCAN	PBE
RPA+RSE	-4.18	-4.03	-5.11	-4.99
RPA	-3.17	-3.30	-3.38	-3.73
DFT	-3.08	1.01	-4.04	1.29
HF+CABS ^b		4.12		
MP2-F12 ^b		-4.30		
CCSD(T) ^c		-4.71		
DMC ^d		-5.3 ± 0.5		

^a RPA correlation energies are extrapolated to the basis set limit (AVTZ→AVQZ). E^{EXX} , E_c^{RSE} , and self-consistent field DFT energies are computed with the AVQZ basis.

^b Supermolecular calculations of the HF and MP2-F12 energies employ the AVQZ orbital basis and augmented five-zeta auxiliary basis sets.

^c Includes the Hartree-Fock estimate of $n > 4$ -body terms (0.01 kcal/mol).

^d Diffusion Monte Carlo, Ref. 24.

ization.

From Table 6 it is clear that the RSE correction in ab initio DFT is still large and necessary to correct for the RPA’s underbinding. For example, while E_c^{RSE} is zero for RPA(HF) by definition,²³ we find that the singles correction is as large as 1.7 kcal/mol for OEPX and 2.4 kcal/mol for OEP2-sc orbitals. We note that, if we take the OEP2-sc as a reference, the mean-field contribution, $E^{\text{HF}} + E_c^{\text{RSE}}$, is significantly better reproduced by (hybrid) GGAs and meta-GGAs than by Hartree-Fock orbitals. The RPA correlation component of the interaction energy, E_c^{RPA} , becomes more attractive as the orbital gap narrows. The largest orbital gap is for the Hartree-Fock reference state, which also underbinds the most. The gap is wide because the exchange operator treats virtual orbitals as interacting with an N -electron system. In OEPX there is still no correlation, but the gap narrows because of the multiplicative KS potential with a proper $-1/r$ asymptote. Finally, adding electron correlation in OEP2-sc further narrows the gap and leads to the most negative E_c^{RPA} in the series. This value is then close to the data obtained using pure functionals. From the difference of

$E_{\text{int}}^{\text{RPA(OEP2-sc)+RSE}}$ and $E_{\text{int}}^{\text{RPA(OEPX)+RSE}}$ we estimate that the appropriate treatment of electron correlation in the input orbitals contributes as much as 2 kcal/mol or 30 % of the total two-body energy in methane clathrate cluster.

3.3.2 Trimers

The three-body nonadditive energies tend to be described inaccurately by DFT approximations and the clathrate cluster is not an exception. Indeed, Table 7 shows that at the self-consistent DFT level the energies behave erratically, for SCAN and SCAN0 the three-body energies are attractive, for PBE and PBE0 they are strongly repulsive. Similar observations have been made by Deible *et al.* in their study.²⁴ Therefore, it is interesting to inspect to what extent is the post-Kohn-Sham RPA sensitive to the inaccuracies in the approximate DFT hamiltonians.

The RPA’s sensitivity to input eigenstates is reflected in the behavior of the E^{HF} component of the RPA interaction energy. Unlike the self-consistent DFT energy, E^{HF} is negative for all orbital inputs, but still varies in magnitude between different models. E^{HF} is negative but close to zero for SCAN0 and equals -4.3 kcal/mol for PBE. While it is the total RPA interaction energy which has a direct physical interpretation, the variance of E^{HF} due to the choice of the semilocal exchange model is an indicator of the quality of the exchange potential model. The variance can be assessed, for example, by comparing the results obtained with pure functional and its hybrid variant. In this regard, the effect is particularly large for the PBE functional, the E^{HF} components of RPA(PBE) and RPA(PBE0) differ by 3 kcal/mol. By contrast, the E^{HF} components of RPA(SCAN) and RPA(SCAN0) are close to each other, which indicates that SCAN orbitals are more robust against the addition of exact exchange.

Adding now the E^{HF} and E_c^{RPA} components together we find that the RPA(PBE) and RPA(PBE0) three-body nonadditive interaction energies have incorrect signs. Moreover, the nonadditive energy of RPA(PBE) exhibits an error of almost 3 kcal/mol. Those errors are

Table 6: Total interaction energies and interaction energy components of 20 dimers $\text{CH}_4 \cdots \text{H}_2\text{O}$. Highest occupied orbital energies and LUMO-HOMO energy differences of various DFT methods, averaged over 20 dimers. The units of interaction energies and orbital energies are kcal/mol and eV, respectively.

	SCAN0 ^a	PBE0 ^a	SCAN ^a	PBE ^a	HF ^a	OEPX ^b	OEP2-sc ^b
RPA+RSE ^c	-5.36	-5.41	-6.46	-6.70	-2.98	-4.47	-6.37
RPA ^d	-4.35	-4.14	-4.43	-3.87	-2.98	-2.77	-3.94
CCSD(T)				-6.31			
E_c^{RPA}	-9.74	-9.77	-11.17	-11.56	-6.81	-8.65	-11.04
$E^{\text{HF}} + E_c^{\text{RSE}}$	4.38	4.36	4.71	4.87	3.83	4.18	4.66
E^{HF}	5.39	5.62	6.74	7.69	3.83	5.88	7.10
CH ₄							
ϵ_{HOMO}	-11.3	-11.0	-9.9	-9.5	-14.9	-14.9	-14.0
$\epsilon_{\text{LUMO}} - \epsilon_{\text{HOMO}}$	11.7	11.1	10.2	9.1	15.6	10.3	10.0
H ₂ O							
ϵ_{HOMO}	-9.3	-9.0	-7.6	-7.2	-13.8	-13.8	-11.2
$\epsilon_{\text{LUMO}} - \epsilon_{\text{HOMO}}$	9.3	8.6	7.2	6.2	14.4	8.2	6.8

^a CBS extrapolation (AVTZ→AVQZ) for the correlation part of the interaction energy; the AVQZ basis for orbital energies.

^b CBS extrapolation (aug-cc-pVDZU→aug-cc-pVTZU) for interaction energies and their components; the aug-cc-pVTZU basis for orbital energies. “U” denotes an uncontracted basis set.

^c Label RPA+RSE denotes the interaction energy $E_{\text{int}}^{\text{RPA+RSE}} = E^{\text{HF}} + E_c^{\text{RSE}} + E_c^{\text{RPA}}$

^d Label RPA denotes the interaction energy $E_{\text{int}}^{\text{RPA}} = E^{\text{HF}} + E_c^{\text{RPA}}$

most likely artifacts of the PBE model. The total three-body nonadditive interaction energies of RPA(HF) are on par with RPA(SCAN) and RPA(SCAN0), underestimating the reference value by around 0.5 kcal/mol.

The RSE-corrected approaches RPA(PBE)+RSE and RPA(PBE0)+RSE are free from the issues described above. For the SCAN-based variants, the singles corrections are small and slightly deteriorate the results. That is consistent with our observations in Ref. 21, where RSE was found to slightly worsen the RPA(SCAN0) energies on the dataset of Řezáč et al.⁵ The results shown here further support the previous recommendation not to use RSE with RPA(SCAN0) when computing three-body energies separately.

Finally, note that the best agreement for the total three-body term is given by

RPA(PBE)+RSE. This is true both for trimers with hydrogen-bonded water molecules (subset 3b 1hb) and trimers with no hydrogen bond (subset 3b 0hb), see Table 8. However, this is rather deceptive, especially for the 3b 0hb subset, where there are both positive and negative errors that mostly cancel out. The mean absolute error (MAE) of RPA(PBE)+RSE for the 3b 0hb subset (equal to 0.0023 kcal/mol) is about twice as large as the MAE of 0.001 kcal/mol obtained both for RPA(PBE0)+RSE and RPA(SCAN0). Also RPA(SCAN) and RPA(HF) show lower MAE values for the 3b 0hb subset, 0.0015 and 0.0017 kcal/mol, respectively.

3.3.3 Tetramers and $n > 4$ -body clusters

The MBE of the methane clathrate is typical of a nonpolar system. Its terms decay fast

Table 7: Nonadditive interaction energies (kcal/mol) of 190 trimers $\text{CH}_4(\text{H}_2\text{O})_2$.

	SCAN0	PBE0	SCAN	PBE	HF
RPA+RSE	0.40	0.74	0.41	0.94	0.53
RPA	0.64	-0.21	0.59	-2.01	0.53
DFT/HF ^a	-0.11	4.39	-0.54	7.45	-0.27
CCSD(T)			1.04		
E_c^{RPA}	0.66	1.46	0.64	2.34	0.81
$E^{\text{HF}} + E_c^{\text{RSE}}$	-0.26	-0.71	-0.23	-1.40	-0.27
E^{HF}	-0.01	-1.67	-0.04	-4.35	-0.27

^a Self-consistent field energies are obtained with the AVQZ basis.

Table 8: Contributions to the methane—water cage interaction energy divided into n -body terms (nb) and subsystems with m hydrogen bonds (mhb). Energies are in kcal/mol.

Method	2b	3b 1hb	3b 0hb	4b 2hb	4b 1hb	4b 0hb	Sum
HF+CABS	3.827	-1.483	1.210	0.164	0.471	-0.083	4.107
CCSD(T)	-6.310	-0.398	1.434	0.056	0.552	-0.051	-4.718
RPA(PBE)	-3.874	-1.849	-0.160	1.152	1.551	0.374	-2.806
RPA(PBE)+RSE	-6.699	-0.470	1.411	0.132	0.705	0.017	-4.904
RPA(PBE0)	-4.142	-1.083	0.872	0.416	0.847	0.055	-3.036
RPA(PBE0)+RSE	-5.409	-0.608	1.349	0.090	0.585	-0.044	-4.038
RPA(SCAN)	-4.433	-0.721	1.316	-0.113	0.539	-0.071	-3.484
RPA(SCAN)+RSE	-6.461	-0.642	1.049	0.208	0.725	0.017	-5.104
RPA(SCAN0)	-4.350	-0.668	1.308	-0.007	0.561	-0.052	-3.208
RPA(SCAN0)+RSE	-5.361	-0.729	1.127	0.162	0.634	-0.026	-4.192
RPA(HF)	-2.983	-0.770	1.303	—	—	—	—

with the number of interacting molecules n . The Hartree-Fock contribution dominates the four-body term and amounts to 0.55 kcal/mol. The five- and higher-body contributions sum up to almost zero at the Hartree-Fock level. The CCSD(T) correlation energy contributes less than 0.01 kcal/mol to the four-body non-additive energy; we assume it to be negligible for $n > 4$.

Taking into account the limited role of electron correlation, it is expected that RPA performs well for $n \geq 4$. Indeed, the best variants overall, RPA(PBE0)+RSE and RPA(SCAN0), deviate from the reference by less than 0.1 kcal/mol for the four-body energy and predict vanishingly small $n > 4$ contributions (Table 9). Therefore, they are consistent with the decay rate of n -body terms shown by the CCSD(T) scheme.

It may appear puzzling why the other RPA variants, i.e., RPA(PBE) and RPA(PBE0), overshoot the four-body energy by more than a factor of two and show large residuals in the $n > 4$ terms. For those methods, the MBE is still not converged after including the four-body terms. A compelling explanation is that, in the PBE description, methane interacts with water molecules which developed too large dipole moments. As reported by Chen *et al.*,⁷¹ PBE overestimates the polarizability of water, which results in bulk waters having excessive dipole moments as compared with experimental reference. See also Ref. 72 and references therein. The SCAN and PBE0 functionals improve the description of water properties.^{71,73} While not so obvious in lower-order terms, the overestimated many-body interactions accumulate in higher-body contributions, as seen in Table 9.

Both the Hartree-Fock mixing and RSE alleviate the problem: the fourth-order MBE for RPA(PBE)+RSE and RPA(PBE0)+RSE are converged to within 0.1 kcal/mol.

In the self-consistent DFT description, the four-body energies have either a wrong sign or a magnitude which is several times too large (Table 9). From the difference between PBE and PBE0 it appears that the errors are mainly due to the PBE exchange. The performance of SCAN is less dependent on the addition of the Hartree-Fock exchange.

Finally, let us discuss the accuracy of RPA for the subsets of four-body terms containing fragments with different number of hydrogen bonds, *i.e.*, subsets 4b 2hb, 4b 1hb, and 4b 0hb (Table 8). On average, RPA(PBE)+RSE gives more repulsive contributions on all three subsets, even though the individual errors are again both positive and negative, see the SI. The magnitude of the errors is consistently reduced upon going to RPA(PBE0)+RSE. RPA(SCAN) and RPA(SCAN0) four-body terms are too attractive overall, which is primarily caused by too attractive energies in the 4b 2hb subset. The errors for the other two subsets are marginal.

Table 9: Four-body and higher-order nonadditive interaction energies (kcal/mol). The four-body energies are sums over 1140 tetramers $\text{CH}_4(\text{H}_2\text{O})_3$.

	SCAN0	PBE0	SCAN	PBE
Four-body nonadditive contributions				
RPA+RSE	0.77	0.63	0.95	0.85
RPA	0.50	1.32	0.35	3.08
DFT ^a	1.35	-1.68	1.94	-3.46
CCSD(T)		0.56		
$n > 4$ -body nonadditive contributions				
RPA+RSE	0.01	0.01	-0.01	-0.09
RPA	0.04	-0.26	0.10	-0.92
DFT ^a	-0.10	0.67	-0.27	1.18
E_c^b	0.00	0.15	-0.05	0.26

^a Self-consistent field energies obtained with the AVQZ basis.

^b RPA correlation energy contribution extrapolated to the basis set limit (AVTZ→AVQZ).

Table 10: Subsets of n -body clusters and the share of electron correlation in their MBE contributions.

Subset	N^a	E_{int}^b	$\left \frac{E_{\text{int,c}}}{E_{\text{int}}}\right ^c$	$\left \frac{E_{\text{disp}}}{E_{\text{int}}}\right ^d$
2b	20	-6.31	1.6	1.8
3b 1hb	30	-0.40	2.7	1.8
3b 0hb	160	1.43	0.2	0.3
4b 2hb	60	0.06	1.9	—
4b 1hb	420	0.55	0.1	—
4b 0hb	660	-0.05	0.6	—

^a Number of clusters in each subset.

^b CCSD(T) reference energy (kcal/mol).

^c $E_{\text{int,c}}$ is the contribution of the coupled-cluster correlation to the (nonadditive) interaction energy.

^d E_{disp} is the dispersion energy. The two-body dispersion energy includes the exchange-dispersion part.

3.3.4 General remarks

The accuracy of RPA for n -body clusters depends on the amount of electron correlation in the MBE term. When the contribution of the correlation energy is significant, the results become strongly dependent on the exchange-correlation model.²¹

Table 10 shows subsets of MBE contributions, presented together with the fraction of the correlation energy. The subsets with a particularly high correlation content are dimers, trimers 1hb, and tetramers 2hb. Indeed, those are the subsets where all RPA methods show the most significant deviations from the reference (Table 8). The remaining cases are subsystems where Hartree-Fock is already qualitatively correct and the correlation part is moderate: 3b 0hb, 4b 1hb, and 4b 0hb. For those systems, the best RPA methods, RPA(SCAN0) and RPA(PBE0)+RSE, reach the accuracy of about 0.1 kcal/mol, which is almost within the uncertainty of the benchmark. For the systems with a moderate amount of correlation RPA falls midway between MP2 and the reference, see Table 8.

3.3.5 Incremental approach

Compared to the leading terms, e.g., dimer energies, the higher n -body nonadditivities require less sophisticated treatment of electron correlation.^{56,74} A frequent practice is to combine the CCSD(T) treatment of dimers with higher-order terms treated at the level of MP2, HF, or force-field.⁷⁴ For clathrate, one can note that the largest RPA errors occur for compact fragments, that is, dimers and also trimers and tetramers with hydrogen bonded water molecules (Table 8). Therefore, a simple way to improve the accuracy of the predicted RPA interaction energies is to replace all or some of these terms with their CCSD(T) counterparts. Let us define the following subsets \mathcal{L}_X of fragments:

$$\begin{aligned}
 \mathcal{L}_0 &= \emptyset \\
 \mathcal{L}_{2b} &= \{2b\} \\
 \mathcal{L}_{3b\ 1hb} &= \{2b, 3b\ 1hb\} \\
 \mathcal{L}_{3b\ 0hb} &= \{2b, 3b\ 1hb, 3b\ 0hb\} \\
 &\vdots \\
 \mathcal{L}_\infty &= \{2b, 3b, 4b, \dots, 21b\}
 \end{aligned} \tag{11}$$

In the last set all the fragments are included. This is equivalent to the supermolecular calculation. In practice, replacing RPA contributions with CCSD(T) for smaller fragments, up to X , can be written in a compact way as

$$\begin{aligned}
 E_{\text{int}}^{\text{CC/RPA},X} &= \\
 &\sum_{\zeta \in \mathcal{L}_X} \left(E_{\text{int}}^{\text{CCSD(T)}}[\zeta] - E_{\text{int}}^{\text{RPA}}[\zeta] \right) + E_{\text{int}}^{\text{RPA}}[\mathcal{L}_\infty]
 \end{aligned} \tag{12}$$

Alternatively, one can view the scheme as combination of CCSD(T) many-body contributions up to X with RPA many-body terms beyond X :

$$\begin{aligned}
 E_{\text{int}}^{\text{CC/RPA},X} &= \\
 &\sum_{\zeta \in \mathcal{L}_X} E_{\text{int}}^{\text{CCSD(T)}}[\zeta] + \sum_{\zeta' \in \mathcal{L}_\infty \setminus \mathcal{L}_X} E_{\text{int}}^{\text{RPA}}[\zeta']
 \end{aligned} \tag{13}$$

The incremental approach obviously works the best when the RPA many-body contribu-

tions are close to the CCSD(T) values. It means that inferior performance can be expected when there is an artificial error cancellation between the different n -body nonadditivities. Moreover, as we deem the CCSD(T) MBE to be essentially converged using four-body terms, within 0.01 kcal/mol, there will be an error in the RPA correction scheme if the five- and higher-body residual terms are significant. This can be seen from Eq. 12: the CC/RPA value for the complete set (up to 4b 0hb) will be the CCSD(T) energy obtained using MBE plus the RPA residual term. The residual terms are particularly large for RPA based on the PBE and PBE0 functionals, being -0.92 and -0.26 kcal/mol, respectively (Table 9). These then cause the erroneous behavior of CC/RPA(PBE) and CC/RPA(PBE0) shown in Figure 3. The RSE corrections reduce the residual terms and error cancellations between n -body contributions, leading to improved performance of the correction scheme for both PBE- and PBE0-based RPA. The error of CC/RPA(PBE0)+RSE is only 4.7 % after replacing the two-body RPA terms with CCSD(T). Subsequent corrections keep the energy within 1.6 % or 0.08 kcal/mol of the reference value.

The SCAN- and SCAN0-based RPA are much less prone to the error cancellations, even without RSE. Also note that the RSE terms degrade the accuracy of the three- and higher-order nonadditive energies. As a consequence one can see that CC/RPA(SCAN) and CC/RPA(SCAN0) without RSE perform somewhat better than the variants with RSE. Overall, the CC/RPA(SCAN0) scheme looks particularly promising. The error is around 3 % or 0.15 kcal/mol when terms up to 3b 1hb are treated with CCSD(T). When the 3b 0hb terms are added, the predicted interaction energy gets within 1 % or 0.05 kcal/mol of the reference.

It is interesting to compare the RPA-based correction scheme to those based on HF and MP2 as well as to standard CCSD(T) MBE. In the last approach, one needs to include explicitly the 4b 1hb term (0.552 kcal/mol) to reduce the error below 10 %. In the clathrate interaction energy, the HF contribution domi-

nates over correlation for all terms above and including 3b 0hb. One can therefore expect that CC/HF, which amounts to starting from the HF supermolecular interaction energy and adding only correlation, will improve the convergence significantly. This is indeed observed (Figure 3) but the partial cancellation of correlation terms between 4b 2hb and 4b 1hb groups means that the error is still around 0.1 kcal/mol even with the 4b 2hb clusters treated at the CCSD(T) level. MP2 lacks accurate description of the three-body correlation and its error is more than two times larger than the error of RPA(PBE0)+RSE for the 3b 1hb and 3b 0hb subsets. Therefore CC/MP2 has larger errors than either CC/RPA(PBE0)+RSE or CC/RPA(SCAN) when these two sets of fragments are not treated explicitly. These three methods show comparable results when even larger clusters are treated explicitly with CCSD(T). However, the cost of RPA calculations grows less steeply than that of MP2 when the system size is increased and precision is not sacrificed. This offers an advantage for the CC/RPA scheme for systems such as molecular solids where converging MP2 with k-points is difficult.^{75,76}

4 Conclusions

We have reported the most accurate to date CCSD(T) estimate of the interaction energy of the methane molecule in a dodecahedral water cage. This reference energy is obtained as a sum of counterpoise-corrected many-body contributions through the four-body terms, with higher-order terms accounted for at the Hartree-Fock level. We have analyzed the convergence of each MBE term with the basis-set cardinal number and compared the canonical and F12 variants of CCSD(T) for additional validation. We used the benchmark data to analyze the performance of Møller-Plesset perturbation theory and post-Kohn-Sham RPA based on orbitals of PBE, SCAN, and the hybrid variants of those functionals.

RPA is known to underestimate noncovalent binding and here we confirm that two-body in-

teractions are the main cause of this error. The RSE correction represents a simple remedy of this problem. This holds for all the tested orbitals: pure and hybrid GGAs and meta-GGAs as well as the orbitals generated with optimized effective potentials (OEPX and OEP2-sc).

Remarkably, the inclusion of singles can also correct wrong signs of three- and four-body nonadditive energies as well as mitigate excessive higher-order contributions to the many-body expansion. This point is particularly relevant for RPA based on the PBE and PBE0 functionals. For a nonpolar system the sum of $n > 4$ -body terms is expected to be negligible, but it is as large as -0.92 kcal/mol and -0.26 kcal/mol for RPA(PBE) and RPA(PBE0), respectively. This erratic behavior is largely corrected by the RSE term.

RPA based on SCAN and SCAN0 eigenstates shows a different behavior compared to RPA based on PBE or PBE0 eigenstates. The nonadditive energies of RPA(SCAN) and RPA(SCAN0) are close to those of RPA(HF). For this reason, the RSE contribution to the $n \geq 3$ -body nonadditivities is smaller than for the PBE-based variants and does not introduce a qualitative change.

Finally, the errors in the RPA interaction energy stem mainly from small compact clusters, *i.e.*, dimers and trimers with hydrogen bonded water molecules. This makes RPA suitable for an incremental approach where CCSD(T) is used for the problematic terms and RPA for the remainder. For example, treating the twenty dimers and thirty hydrogen-bonded trimers at the CCSD(T) level and using RPA(PBE0)+RSE for the rest, the incremental interaction energy lies within 0.08 kcal/mol of the reference. This represents an error of only 1.6 % and makes this scheme promising for treatment of larger clusters and solids.

Acknowledgement This work was supported by the European Research Council (ERC) under the European Union’s Horizon 2020 research and innovation program (grant agreement No 759721) and by the Primus programme of the Charles University. S.Š. is

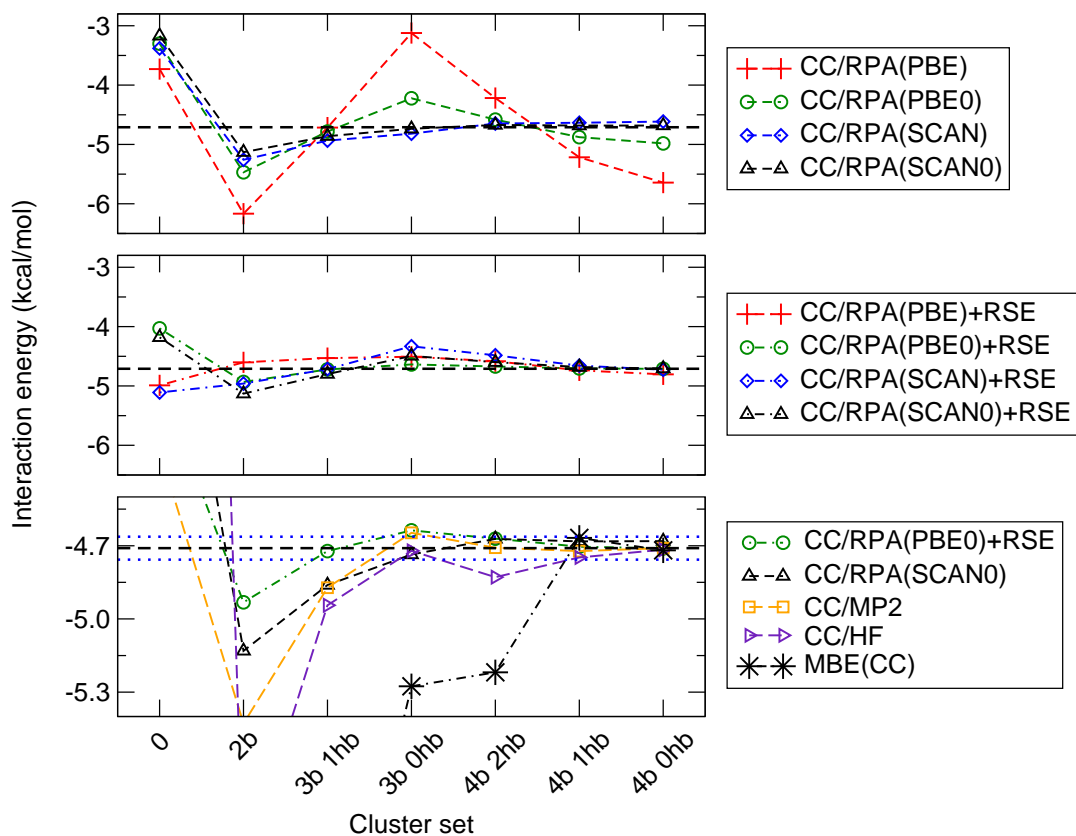


Figure 3: Methane—water cage interaction energy in the incremental approach based on RPA (top panel) and RPA+RSE (middle panel). The bottom panel compares the two best CC/RPA approaches (CC/RPA(PBE0)+RSE and CC/RPA(SCAN0)) to MBE at the CCSD(T) level and the correction scheme based on HF and MP2. On x axis we give the index of cluster subset \mathcal{L}_X up to which CCSD(T) calculations are performed. In the bottom panel, the dashed line denotes the reference value of -4.71 kcal/mol and the blue dotted lines are placed at values one percent above and below the reference.

grateful to the Polish National Science Center for the partial financial support under Grant No. 2016/21/D/ST4/00903. This research was supported in part by PLGrid Infrastructure. We are also grateful for computational resources provided by the IT4Innovations National Supercomputing Center (LM2015070), CESNET (LM2015042), CERIT Scientific Cloud (LM2015085), and e-Infrastruktura CZ (e-INFRA LM2018140). The authors thank Prof. Grzegorz Chałasiński for useful discussions related to this work.

Supporting Information Available

The following files are available free of charge. Spreadsheets with raw numerical data and computational details, geometries in a form of xyz files. The supporting information is available free of charge via the Internet at publisher's website.

References

- (1) Jurecka, P.; Sponer, J.; Cerny, J.; Hobza, P. *Phys. Chem. Chem. Phys.* **2006**, *8*, 1985–1993.
- (2) Peverati, R.; Truhlar, D. G. *Phil. Trans. R. Soc. A* **2014**, *372*, 20120476.
- (3) Taylor, D. E.; Ángyán, J. G.; Galli, G.; Zhang, C.; Gygi, F.; Hirao, K.; Song, J. W.; Rahul, K.; Anatole von Lilienfeld, O.; Podeszwa, R.; Bulik, I. W.; Henderson, T. M.; Scuseria, G. E.; Toulouse, J.; Peverati, R.; Truhlar, D. G.; Szalewicz, K. *J. Chem. Phys.* **2016**, *145*, 124105.
- (4) Goerigk, L.; Hansen, A.; Bauer, C.; Ehrlich, S.; Najibi, A.; Grimme, S. *Phys. Chem. Chem. Phys.* **2017**, *19*, 32184–32215.
- (5) Rezac, J.; Huang, Y.; Hobza, P.; Beran, G. J. *J. Chem. Theory Comput.* **2015**, *11*, 3065.
- (6) Huang, Y.; Beran, G. J. O. *J. Chem. Phys.* **2015**, *143*, 044113.
- (7) Jankiewicz, W.; Podeszwa, R.; Witek, H. A. *J. Chem. Theory Comput.* **2018**, *14*, 5079–5089.
- (8) Lotrich, V. F.; Szalewicz, K. *Phys. Rev. Lett.* **1997**, *79*, 1301.
- (9) Yang, J.; Hu, W.; Usvyat, D.; Matthews, D.; Schütz, M.; Chan, G. K.-L. *Science* **2014**, *345*, 640–643.
- (10) Kennedy, M. R.; McDonald, A. R.; DePrince, A. E.; Marshall, M. S.; Podeszwa, R.; Sherrill, C. D. *J. Chem. Phys.* **2014**, *140*, 121104.
- (11) Gillan, M. *J. Chem. Phys.* **2014**, *141*, 224106.
- (12) Hapka, M.; Rajchel, L.; Modrzejewski, M.; Schaeffer, R.; Chalasinski, G.; Szczesniak, M. M. *J. Chem. Phys.* **2017**, *147*, 084106.
- (13) Eshuis, H.; Bates, J. E.; Furche, F. *Theor. Chem. Acc.* **2012**, *131*, 1084.
- (14) Richard, R. M.; Lao, K. U.; Herbert, J. M. *Acc. Chem. Res.* **2014**, *47*, 2828–2836.
- (15) Eshuis, H.; Yarkony, J.; Furche, F. *J. Chem. Phys.* **2010**, *132*, 234114.
- (16) Kaltak, M.; Klimes, J.; Kresse, G. *J. Chem. Theory Comput.* **2014**, *10*, 2498.
- (17) Kaltak, M.; Klimes, J.; Kresse, G. *Phys. Rev. B* **2014**, *90*, 054115.
- (18) Schurkus, H. F.; Ochsenfeld, C. *J. Chem. Phys.* **2016**, *144*, 031101.
- (19) Wilhelm, J.; Seewald, P.; Del Ben, M.; Hutter, J. *J. Chem. Theory Comput.* **2016**, *12*, 5851.
- (20) Klimeš, J. *J. Chem. Phys.* **2016**, *145*, 094506.
- (21) Modrzejewski, M.; Yourdkhani, S.; Klimes, J. *J. Chem. Theory Comput.* **2020**, *16*, 427–442.
- (22) Ren, X.; Rinke, P.; Scuseria, G. E.; Scheffler, M. *Phys. Rev. B* **2013**, *88*, 035120.
- (23) Klimes, J.; Kaltak, M.; Maggio, E.; Kresse, G. *J. Chem. Phys.* **2015**, *143*, 102816.
- (24) Deible, M. J.; Tuguldur, O.; Jordan, K. D. *J. Phys. Chem. B* **2014**, *118*, 8257–8263.
- (25) Cox, S. J.; Towler, M. D.; Alfè, D.; Michaelides, A. *J. Chem. Phys.* **2014**, *140*, 174703.
- (26) Gill, P. M.; Johnson, B. G.; Pople, J. A.; Frisch, M. J. *Chem. Phys. Lett.* **1992**, *197*, 499–505.
- (27) Perdew, J.; Burke, K.; Ernzerhof, M. *Phys. Rev. Lett.* **1996**, *77*, 3865–3868.
- (28) Dubecký, M.; Jurečka, P.; Mitas, L.; Ditte, M.; Fanta, R. *J. Chem. Theory Comput.* **2019**, *15*, 3552–3557.

- (29) Lao, K. U.; Herbert, J. M. *J. Chem. Theory Comput.* **2018**, *14*, 5128–5142.
- (30) Riplinger, C.; Sandhoefer, B.; Hansen, A.; Neese, F. *J. Chem. Phys.* **2013**, *139*, 134101.
- (31) Liakos, D. G.; Sparta, M.; Kesharwani, M. K.; Martin, J. M.; Neese, F. *J. Chem. Theory Comput.* **2015**, *11*, 1525–1539.
- (32) Werner, H.-J.; Knowles, P. J.; Knizia, G.; Manby, F. R.; Schütz, M. *WIREs Comput. Mol. Sci.* **2012**, *2*, 242–253.
- (33) Kendall, R. A.; Dunning Jr, T. H.; Harrison, R. J. *J. Chem. Phys.* **1992**, *96*, 6796–6806.
- (34) Schuchardt, K. L.; Didier, B. T.; Elsethagen, T.; Sun, L.; Gurumoorthi, V.; Chase, J.; Li, J.; Windus, T. L. *J. Chem. Inf. Model.* **2007**, *47*, 1045–1052.
- (35) Halkier, A.; Klopper, W.; Helgaker, T.; Jørgensen, P.; Taylor, P. R. *J. Chem. Phys.* **1999**, *111*, 9157–9167.
- (36) Werner, H.-J.; Adler, T. B.; Manby, F. R. *J. Chem. Phys.* **2007**, *126*, 164102.
- (37) Adler, T. B.; Knizia, G.; Werner, H.-J. *J. Chem. Phys.* **2007**, *127*, 221106.
- (38) Knizia, G.; Adler, T. B.; Werner, H.-J. *J. Chem. Phys.* **2009**, *130*, 054104.
- (39) Noga, J.; Šimunek, J. *Chem. Phys.* **2009**, *356*, 1–6.
- (40) Weigend, F. *Phys. Chem. Chem. Phys.* **2002**, *4*, 4285–4291.
- (41) Weigend, F.; Köhn, A.; Hättig, C. *J. Chem. Phys.* **2002**, *116*, 3175–3183.
- (42) Weigend, F.; Ahlrichs, R. *Phys. Chem. Chem. Phys.* **2005**, *7*, 3297–3305.
- (43) Yousaf, K. E.; Peterson, K. A. *Chem. Phys. Lett.* **2009**, *476*, 303–307.
- (44) Talman, J. D.; Shadwick, W. F. *Phys. Rev. A* **1976**, *14*, 36–40.
- (45) Grabowski, I.; Fabiano, E.; Teale, A. M.; Šmiga, S.; Buksztel, A.; Sala, F. D. *J. Chem. Phys.* **2014**, *141*, 024113.
- (46) Šmiga, S.; Grabowski, I.; Witkowski, M.; Musard, B.; Toulouse, J. *J. Chem. Theory Comput.* **2020**, *16*, 211–223.
- (47) Šmiga, S.; Marusiak, V.; Grabowski, I.; Fabiano, E. *J. Chem. Phys.* **2020**, *152*, 054109.
- (48) Šmiga, S.; Constantin, L. A. *J. Phys. Chem. A* **2020**, *124*, 5606–5614.
- (49) Stanton, J. F.; Gauss, J.; Watts, J. D.; Noojien, M.; Oliphant, N.; Perera, S. A.; Szalay, P.; Lauderdale, W. J.; Kucharski, S.; Gwaltney, S.; Beck, S.; Balková, A.; Bernholdt, D. E.; Baeck, K. K.; Rozyczko, P.; Sekino, H.; Hober, C.; R. J. Bartlett Integral packages included are VMOL (J. Almläf and P.R. Taylor); VPROPS (P. Taylor) ABACUS; (T. Helgaker, H.J. Aa. Jensen, P. Jørgensen, J. Olsen, and P.R. Taylor), *ACES II*; Quantum Theory Project: Gainesville, Florida, 2007.
- (50) Šmiga, S.; Fabiano, E. *Phys. Chem. Chem. Phys.* **2017**, *19*, 30249–30260.
- (51) Görling, A. *Phys. Rev. Lett.* **1999**, *83*, 5459–5462.
- (52) Ivanov, S.; Hirata, S.; Bartlett, R. J. *Phys. Rev. Lett.* **1999**, *83*, 5455–5458.
- (53) Hirata, S.; Ivanov, S.; Grabowski, I.; Bartlett, R. J.; Burke, K.; Talman, J. D. *J. Chem. Phys.* **2001**, *115*, 1635–1649.
- (54) Ivanov, S.; Hirata, S.; Bartlett, R. J. *J. Chem. Phys.* **2002**, *116*, 1269–1276.
- (55) Richard, R. M.; Lao, K. U.; Herbert, J. M. *J. Chem. Phys.* **2014**, *141*, 014108.
- (56) Góra, U.; Podeszwa, R.; Cencek, W.; Szalewicz, K. *J. Chem. Phys.* **2011**, *135*, 224102.
- (57) Marchetti, O.; Werner, H.-J. *J. Phys. Chem. A* **2009**, *113*, 11580–11585.
- (58) Pitoňák, M.; Neogrády, P.; Černý, J.; Grimme, S.; Hobza, P. *ChemPhysChem* **2009**, *10*, 282–289.
- (59) Axilrod, B. M.; Teller, E. *J. Chem. Phys.* **1943**, *11*, 299–300.
- (60) Muto, Y. *J. Phys. Math. Soc. Japan* **1943**, *17*, 629.
- (61) Outputs of calculations and processing script. https://github.com/klimes/Clathrate_cluster_data.
- (62) Valiron, P.; Mayer, I. *Chem. Phys. Lett.* **1997**, *275*, 46–55.
- (63) Walczak, K.; Friedrich, J.; Dolg, M. *J. Chem. Phys.* **2011**, *135*.
- (64) Richard, R.; Lao, K.; Herbert, J. *J. Phys. Chem. Lett.* **2013**, *4*, 2674–2680.
- (65) Ouyang, J. F.; Bettens, R. P. A. *J. Chem. Theory Comput.* **2015**, *11*, 5132–5143.

- (66) Liu, K.-Y.; Herbert, J. *J. Chem. Phys.* **2017**, *147*.
- (67) Richard, R.; Bakr, B.; Sherrill, C. *J. Chem. Theory Comput.* **2018**, *14*, 2386–2400.
- (68) Peyton, B.; Crawford, T. *J. Phys. Chem. A* **2019**, *123*, 4500–4511.
- (69) Parrish, R. M.; Hohenstein, E. G.; Sherrill, C. D. *J. Chem. Phys.* **2013**, *139*, 174102.
- (70) Bartlett, R. J. *Mol. Phys.* **2010**, *108*, 3299–3311.
- (71) Chen, M.; Ko, H.-Y.; Remsing, R. C.; Andrade, M. F. C.; Santra, B.; Sun, Z.; Selloni, A.; Car, R.; Klein, M. L.; Perdew, J. P.; Wu, X. *Proc. Natl. Acad. Sci. U. S. A.* **2017**, *114*, 10846–10851.
- (72) Gillan, M. J.; Alfe, D.; Michaelides, A. *J. Chem. Phys.* **2016**, *144*, 130901.
- (73) Adamo, C.; Cossi, M.; Scalmani, G.; Barone, V. *Chem. Phys. Lett.* **1999**, *307*, 265–271.
- (74) Wen, S.; Nanda, K.; Huang, Y.; Beran, G. J. O. *Phys. Chem. Chem. Phys.* **2012**, *14*, 7578–7590.
- (75) Del Ben, M.; Hutter, J.; VandeVondele, J. *J. Chem. Theory Comput.* **2013**, *9*, 2654–2671.
- (76) Liao, K.; Grüneis, A. *J. Chem. Phys.* **2016**, *145*, 141102.